Importance of the Q/N-rich Segment for Protein Stability and Activity of Endogenous Mouse TDP-43

Toshiya Sato (serendip@med.kitasato-u.ac.jp)
Kitasato University School of Medicine
Kanako Oda
Niigata University
Seiko Sakai
Niigata University
Rika Kato
Kitasato University School of Medicine
Saori Yamamori
Kitasato University School of Medicine
Makoto Itakura
Kitasato University School of Medicine
Yoshio Kodera
Kitasato University School of Science
Masatoyo Nishizawa
Niigata University of Health and Welfare
Toshikuni Sasaoka
Niigata University
Osamu Onodera
Niigata University
Minesuke Yokoyama
Central Institute for Experimental Animals

Research Article

Keywords: Protein Stability, Endogenous Mouse, molecular pathogenesis

Posted Date: December 6th, 2021

DOI: https://doi.org/10.21203/rs.3.rs-1113360/v1

Abstract

TAR DNA-binding protein 43 kDa (TDP-43), a nuclear protein, plays an important role in the molecular pathogenesis of amyotrophic lateral sclerosis (ALS). TDP-43 aggregation and translocation out of the nucleus are crucial factors in ALS. TDP-43 aggregation results from its resistance to degradation, to which the long-disordered C-terminal region (CTR) is thought to contribute. The CTR has two Gly, aromatic, and Ser-rich (GaroS) segments and an amyloidogenic core divided into a hydrophobic patch and a Gln/Asn (Q/N)-rich segment. Although TDP-43 lacking the CTR is known to be unstable, as observed in knock-in mice, it is unclear which of these segments contributes to the stability of TDP-43. Here, we generated 12 mouse lines lacking the various sub-regions of CTR by genome editing and compared the protein stability, activity, and subcellular localization of TDP-43. We demonstrated the functional diversity of the four segments of CTR, finding that the presence of Q/N-rich segment greatly restored the protein stability and activity of TDP-43. In addition, we found that the second GaroS deletion did not affect protein stability and mouse development.

Introduction

TAR DNA-binding protein 43 kDa (TDP-43), a member of the heterogeneous nuclear ribonucleoprotein family, has emerged as a key player in the molecular pathogenesis of amyotrophic lateral sclerosis (ALS)[1,2]. TDP-43 mainly localizes in the nucleus and is involved in RNA metabolism, including splicing, that promotes cystic fibrosis transmembrane conductance regulator (CFTR) exon 9 skipping[3]. Moreover, TDP-43 is essential for mouse development[4–6]. In ALS, cytoplasmic aggregation of TDP-43 is a pathological feature that is often accompanied by nuclear loss of TDP-43[7,8]. Because the amount of nuclear TDP-43 is strictly regulated by binding of TDP-43 to the 3'-untranslated region of its own mRNA, thereby forming an autoregulatory negative feedback loop[9–13], nuclear loss of TDP-43 can induce the upregulation of TDP-43 mRNA and produce a vicious cycle that leads to the perturbation of TDP-43 homeostasis[14,15]. This imbalance of aggregation-prone TDP-43 plays a role in the pathological mechanism of ALS.

A long-disordered C-terminal region (CTR), known as a prion-like domain[2], is also thought to be important for the stability of TDP-43 and its resistance to degradation. The CTR can be divided into four sub-regions, including a first Gly, aromatic, and Ser-rich (GaroS1) segment; a hydrophobic patch (HP); a Gln/Asn (Q/N)-rich segment; and a second GaroS2 segment (Fig. 1)[16,17]. In the CTR, an amyloidogenic core of amino acid (aa) residues 311–360 has been identified to be critical for aggregation[16]. In addition, the CTR is a hotspot for ALS-causing *TARDBP* mutations. These mutations accelerate aggregate formation, with the result that fragmented and phosphorylated C-termini of TDP-43 accumulate in the affected tissues of ALS patients[18–20]. Recently, TDP-ΔC (aa 274–414) knock-in mice were generated, and they showed embryonic lethality of homozygous mice, and that TDP-43 lacking CTR is unstable[21]. However, it is unclear which of the segments of the CTR contribute to the stability of TDP-43, indicating the importance of analyzing mice with deletions of more localized regions within the CTR. In this study,

we generated 12 mouse lines lacking the various sub-regions of the CTR by genome editing and examined their effects on protein stability, activity, and subcellular localization of TDP-43 to clarify the functional diversity of the C-terminal sub-regions.

Results

Protein stability and activity restoration are dependent on the length of the TDP-43 CTR.

To determine the segment necessary to avoid embryonic lethality of TDP-ΔC knock-in mice[21], we established 12 mouse lines using the zinc finger nuclease (ZFN) and CRISPR/Cas9 systems, which were used to target the Q/N-rich (N345–Q346) and GaroS2 (Y374) segments, respectively (Fig. 1, Supplementary Figs. S1, S2). The 12 mouse lines were categorized into five groups based on the putative protein structures in the CTR (Fig. 1): (1) deletion within a 6-aa region of the Q/N-rich segment (ZE13A/Δ9 and ZE13B/Δ18), (2) deletion within a 6-aa region of the GaroS2 segment (CRY9A/Δ3 and CRY8A/Δ18), (3) frame-shift deletions of the GaroS2 segment (CRY8B/Δ8, CRY9B/Δ29), (4) deletion of most of Q/N-GaroS2 (ZE10/Δ10, ZM39P/Δ295, and ZM87/Δ2), and (5) a large deletion including the GaroS1-HP segment (ZM39A/Δ261). All heterozygous mice were fertile and showed no obvious motor phenotypes during daily handling. Heterozygous intercrosses of each mouse line showed that homozygous mice were viable in Groups 1, 2, and 3, whereas they were embryonic lethal in Groups 4 and 5 (Table 1). Since embryonic lethality was recovered in Group 3 compared to Groups 4 and 5, the GaroS1-HP-Q/N-rich segment is thought to be necessary and sufficient for mouse development.

Table 1
Genotypes of offspring from heterozygous intercrosses. NM, natural mating. IVF, *in vitro* fertilization and embryo transfer. n/a, not applicable. *$p < 0.05$, **$p < 0.01$ (chi-square test).

Group	Mouse line	Mating	Stage	No. of mice with indicated genotype			No. of empty deciduae	No. of resorbed or dead fetuses
				+/+	+/Δ	Δ/Δ		
1	ZE13A/Δ9	NM	Pup	11	19	11	n/a	n/a
	ZE13B/Δ18	NM	Pup	11	20	5	n/a	n/a
2	CRY9A/Δ3	NM	Pup	13	27	12	n/a	n/a
	CRY8A/Δ18	NM	Pup	10	27	11	n/a	n/a
3	CRY8B/Δ8	NM	Pup	19	40	14	n/a	n/a
	CRY9B/Δ29	NM	Pup	19	39	15	n/a	n/a
4	ZE10/Δ10	NM	Pup	11	22	0**	n/a	n/a
		IVF	E12.5	10	20	0**	20	n/a
	M39P/Δ295	IVF	E12.5	7	11	0*	8	n/a
	ZM87/Δ2	NM	Pup	9	13	0*	n/a	n/a
		IVF	E19.5	10	22	0**	90	8 (Δ/Δ: 6)
		IVF	E16.5	2	11	4	11	2 (Δ/Δ: 2)
		IVF	E12.5	6	9	5	4	n/a
5	ZM39A/Δ261	NM	Pup	5	10	0	n/a	n/a
		IVF	E12.5	12	28	0**	22	n/a

To estimate the stability of mutant proteins, we performed subcellular fractionation of eight-week-old mouse cerebrum and western blot analysis using the N-260 anti-TDP-43 antibody. In Group 1 homozygous mice, mutant TDP-43 was observed mainly in the nucleus with a mobility shift consistent with a 3 or 6 aa deletion (Fig. 2a). In Group 3 heterozygous and homozygous mice, the intensity of the band corresponding to the GaroS2 deletion was comparable to that of wild-type (WT) TDP-43 depending on the number of alleles (Fig. 2b). However, mutant bands corresponding to most of the Q/N-GaroS2 deletion were not observable in the nuclear or cytoplasmic fractions of Group 4 heterozygous mice

(Fig. 2c). Because protein stability was restored in Group 3 compared to Group 4, similar to embryonic lethality, the Q/N-rich segment is required for TDP-43 stability and activity.

We noted that the timing of embryonic lethality was different in Group 4 mice (Table 1). The homozygous ZE10/Δ10 and ZM39P/Δ295 mice died before embryonic day (E) 12.5, similar to the previously described TDP-43 knock-out mice[4–6], whereas ZM87/Δ2 mice died between E12.5 and E19.5, showing a variety of phenotypes including resorbed, macerated, anencephalic, or dead fetuses (Supplementary Fig. S3a). These results indicate that TDP-43 lacking most of Q/N-GaroS2 has residual activity only in ZM87/Δ2 mice. Thus, we evaluated cerebellar tissue from ZM87/Δ2 mice at E19.5 and detected weaker bands both in heterozygotes and homozygotes compared to those of WT (Supplementary Fig. S3b). Furthermore, the ZM39P/Δ295 band was detected in unfertilized oocytes at an intensity that was comparable to those of WT and the ZM39A/Δ261 bands (Supplementary Fig. S3c), suggesting that TDP-43 lacking most of Q/N-GaroS2 is rapidly degraded in the cerebrum at eight weeks of age.

The GaroS2 segment negatively regulates its own activity.

Since TDP-43 strictly regulates its own mRNA levels through autoregulation[9–13], its residual activity can be estimated by evaluating its own mRNA level. Thus, we performed qRT-PCR analysis using the following five primer sets: *Hprt1* (internal reference), λpolyA (external control), *Tardbp* exon 3 to 4 (Exon 3–4), *Tardbp* exon 5 to 6 (Exon 5–6), and *Tardbp* exon 6 (WT Exon 6). Exon 3–4 and Exon 5–6 recognize both WT and mutant alleles, whereas one of the WT Exon 6 primers targets deleted sequences induced by genome editing, thus WT Exon 6 recognizes the WT allele alone. In Group 1 homozygous mice, the total expression levels of *Tardbp* mRNA did not change in comparison with those of WT mice (Fig. 2d). However, the total expression levels were significantly increased in Groups 3 (1.247 to 1.448) and 5 (1.853 to 1.974), indicating compensation for the decrease in TDP-43 autoregulatory activity. In sharp contrast, the total expression levels in both Group 4 heterozygotes and homozygotes were significantly decreased (0.850 to 0.887) compared to those of WT mice (Fig. 2e). These results suggest that the residual activity of mutant TDP-43 is increased due to the deletion of the GaroS2 segment, which presumably acts as a negative regulator.

CTR contributes to nuclear localization.

As shown in Fig. 2c, Group 5 heterozygous mice (ZM39A/Δ261) exhibited a strong signal for non-functional TDP-43 lacking the GaroS1-HP segment, which was detected in the cytoplasmic fraction. Although the non-functional TDP-43 had a bipartite nuclear localization signal (NLS, aa 82–98, Fig. 1)[22,23], it was not observed in the nuclear fraction. We performed immunohistochemical analysis of the spinal anterior horn region stained with N-260 anti-TDP-43 antibody, but the mis-localization of mutant TDP-43 was not detected (Fig. 3a). To confirm whether a similar result occurs in human TDP-43, we performed transient expression analysis using HeLa cells with enhanced green fluorescent protein (EGFP) tagged to the N-terminus of human TDP-43 constructs lacking the GaroS1 segment (dGaroS1), a region equivalent to ZM39A/Δ261 (d261CTR) and the entire CTR (dCTR) (Fig. 3b). Similar to the mouse

immunohistochemical analysis, three mutant and WT TDP-43s were localized in the nuclei of living cells, whereas EGFP alone was diffusely localized in cell bodies (Fig. 3c). In contrast to the fluorescence imaging, subcellular fractionation followed by western blotting showed that the three mutant TDP-43s were strongly detected in the cytoplasmic fraction (Fig. 3d). Although the reason is unclear, a similar discrepancy has been reported using constructs with a near total deletion of CTR (aa 314–414)[23,24]. Taking these reports into account, large deletions of CTR appear to disturb the nuclear localization only when assessed by subcellular fractionation and western blotting.

Discussion

We established 12 mouse lines lacking various TDP-43 C-terminal sub-regions and demonstrated that extending the length of CTR to the GaroS1-HP-Q/N-rich segment restored the protein stability and activity of TDP-43. On the other hand, non-functional TDP-43 lacking GaroS1-HP segment was stably expressed and detected in the cytoplasmic fraction, indicating that the stability of TDP-43 does not just depend on its activity. The TDP-ΔC protein is known to be unstable in knock-in mice[21]. Moreover, mammalian TDP-43 genes undergo alternative splicing to produce TDP-43 lacking most of the CTR, namely mTDP-S[25]. Our results strongly suggest that mTDP-Ss are rapidly degraded in the cerebrum. In addition to protein stability, we found that the GaroS2 segment is not essential, but potentially acts as a negative regulator of its own autoregulatory activity.

The protein structure in solution exhibits two canonical α-helices (321–330 and 335–343) in the HP segment[16], which overlaps a highly conserved region (CR, 320-340) flanked by two intrinsically disordered regions (IDR1 and IDR2)[26]. Hydrophobic residues (V, L, I, M, F, Y, and W) in the IDRs are distributed at conserved intervals across vertebrate TDP-43 homologues. These regions are cooperatively involved in liquid-liquid phase separation (LLPS) and forming membraneless organelles[27–29]. The self-association of CTR is synergistic and forms a continuum of physical states, which is proposed to be mainly facilitated by four interacting regions in the GaroS1-HP-Q/N-rich segment, α-helices (aa 321–330), a low complexity aromatic-rich kinked segment (LARKS, aa 312–317), a steric zipper (aa 328–333), and a fibril core (aa 331–360)[30,31]. In contrast, the GaroS2 segment is not necessary for full-length TDP-43 aggregation[32]. These observations suggest that the basic elements necessary for functional LLPS are the GaroS1-HP-Q/N-rich segment.

It has been shown that removing the GaroS2 segment has no apparent effect on either the TDP-43 activity of CFTR exon 9 skipping or intra-cellular localization in cultured cells[23,33]. These reports support our results showing no apparent phenotype in CRY9B/Δ29 mice lacking the GaroS2 segment. However, there are several mutations in the GaroS2 segment that cause familial ALS, and the Y374X mutation, similar to the CRY9B/Δ29 mutation, has been found in sporadic ALS[34]. Furthermore, two steric zippers (aa 370–375 and 396–402) are present in the GaroS2 segment[30]. It is noteworthy that the GaroS2 segment is subjected to phosphorylation at a minimum of seven serine residues (aa 389, 393, 395, 403, 404, 409, and 410)[18–20], which may serve to prevent excessive aggregation[31]. Considering that

disordered proteins are generally regulated by post-translational modifications (PTMs)[35], it may be that the GaroS2 segment is not essential for basic TDP-43 activity, but rather regulates its own activity, presumably due to PTMs including phosphorylation.

We used western blotting to show that human TDP-43 with larger CTR deletions localized mainly in the cytoplasmic fraction, whereas the protein constructs were present in the nuclei of living cells when imaged using fluorescence microscopy. In a pioneering study using U2OS cells and CTR deletion constructs, the observed immunofluorescence patterns of subcellular localizations were variable, whereas biochemical fractionation showed that cytoplasmic localization was dependent on the length of the CTR deletion[23]. Recently, TDP-43 was reported to demix in the cytoplasm as well as the nucleus using CTR[36]. The demixing of RNA-free TDP-43 in the nucleus induces anisotropic intranuclear liquid spherical shells (anisosomes), and the role of the demixing is speculated to tether RNA binding proteins, including TDP-43, near the site of transcription[37]. Furthermore, a nuclear export signal (aa 239–250) in TDP-43 appears to be non-functional, and a significant amount of TDP-43 is exported to cytoplasm through passive diffusion[38,39]. These observations raise the possibility that TDP-43 with large CTR deletions can be imported to the nucleus, but leak out during biochemical fractionation due to insufficient nuclear retention. Although further analysis and mouse models are required to understand the full functional diversity of the TDP-43 C-terminal sub-regions, we expect that the results presented here will help elucidate the pathogenesis of ALS and perhaps lead to the development of new ALS treatments.

Methods

Generation of ZE, ZM, and CRY mouse lines.

CompoZr Custom ZFNs (Sigma-Aldrich, St. Louis, MO) were designed to target *Tardbp* exon 6 and manufactured as ZFN binding (uppercase) and cutting (lowercase) sites (GTTAGCCAGCCAGCAGaaccagTCGGGCCCATCTGGGA). The ZFN mRNAs were microinjected into the pronuclei of B6C3F1/Jcl fertilized oocytes to generate ZE lines according to the manufacturer's instructions. Next, a ssDNA oligonucleotide (Supplementary Fig. S1a) was co-injected with the ZFN mRNAs as a donor template to generate the ZM lines carrying large deletions.

To generate GaroS2-deficient mice, the guide RNA (gRNA) target sequence (TCTGGAAATAATTCCTACAGtgg, lowercase indicating protospacer adaptor motif, PAM) was designed to target *Tardbp* exon 6 encoding the N-terminal region of the GaroS2 segment. The gRNA was synthesized commercially (Thermo Fisher Scientific, Waltham, MA). The gRNA and CAS9 protein (Integrated DNA Technologies, Coralville, IA) were electroporated in fertilized zygotes of C57BL/6JJcl mice using previously described methods with minor modifications[40]. Electroporation was performed in HEPES-buffered Whitten's medium using platinum plate electrodes on tempered glass (LF501PT-1; BEX, Tokyo, Japan). The pulse conditions of CUY21EDIT II (BEX) were 30 V (3 ms pulse duration, 97 ms interval) × 7 times. After electroporation, zygotes were incubated in Whitten's medium for 24 h at 37°C and 5% CO_2,

and the surviving two-cell-stage embryos were transferred into the oviducts of pseudo-pregnant female mice.

The genome-edited founder mice were crossed with C57BL/6JJcl mice to obtain heterozygous mouse lines. The genotyping conditions are described in Supplementary Table S1. All animal experiments were carried out in accordance with the guidelines of the National Institutes of Health, and the Ministry of Education, Culture, Sports, Science and Technology (MEXT) of Japan, and were approved by the Dean of Kitasato University School of Medicine based on judgment by the Institutional Animal Care and Use Committee (Approval no. 2020-061) in compliance with ARRIVE guidelines (https://arriveguidelines.org). All mice were maintained under specific pathogen-free conditions with free access to CE-2 standard food (CLEA, Tokyo, Japan) and ultrafiltered water. For the mouse lines where embryonic lethality was expected, including ZM39P/Δ295, the analysis at E12.5 was prioritized to reduce the number of mice.

Subcellular fractionation and western blotting.

Cerebrum samples from eight-week-old mice were homogenized and divided into four subcellular fractions enriched with cytoplasmic (C), membrane (M), nuclear (N), or insoluble (I) proteins using EzSubcell Extract (WSE-7421, ATTO, Tokyo, Japan). The fractions (C, N, and I), 3 μg per lane, were subjected to western blotting as described previously[41]. The blots were subsequently incubated with the following antibodies: TDP-43 (1:2000, 10782-2-AP, Proteintech, Chicago, IL), α-tubulin (1:5000, T5168, Sigma-Aldrich), or p84 (1:1000, ab131268, Abcam, Cambridge, UK). For subcellular fractionation of cultured cells, the Pierce NE-PER reagents (Thermo Fisher Scientific) were applied according to the method used by Nonaka et al.[24], and antibodies for p84 (1:1000, GTX70220, GeneTex, Irvine, CA) and GFP (1:1000, sc-9996, Santa Cruz Biotechnology, Dallas, TX) were used for detection.

Total RNA preparation and qRT-PCR analysis.

To monitor the measurement process, we spiked external RNA (λpolyA$^+$ RNA-A) from an External Standard Kit for qPCR (Takara, Shiga, Japan) into the cerebral homogenate at a concentration of 1.8×10^6 copies/mg brain tissue, and simultaneously extracted total RNA from the cerebrum using RNAiso Plus (Takara). First-strand cDNA was synthesized using a SuperScript VILO cDNA synthesis Kit (Invitrogen, Waltham, MA). Real-time qRT-PCR was performed using SYBR Premix Ex Taq II and a Thermal Cycler Dice Real-time System (Takara). Each cDNA sample was measured in duplicate applying the ΔΔCT method. Statistical analyses were performed using the REST2009 program (http://www.gene-quantification.de/rest-2009.html). The primer sets are listed in Supplementary Table S1.

Immunohistochemistry.

Immunohistochemical analysis was performed as described previously[42]. Paraffin-embedded 3-μm-thick sections were subjected to immunostaining with N-260 anti-TDP-43 antibody (1:5000, 10782-2-AP, Proteintech). Immunofluorescence images were obtained using Alexa Fluor 488 goat anti-rabbit IgG (1:2000, A11034, Invitrogen) and a LSM710 confocal laser microscope (Carl Zeiss, Jena, Germany).

Cell culture and fluorescence imaging.

WT human TDP-43 cloned into the pEGFP-C3 vector (Clontech, now Takara) was constructed previously[43]. Deletion constructs were generated with a PrimeSTAR Mutagenesis Basal Kit (Takara) using the following primers: for dGaroS1, 5'-TGCCGAAATTAATCCAGCCATGATG-3' and 5'-GGATTAATTTCGGCATTGGATATATG-3'; for d261CTR, 5'-TGCCGAACCATCGGGTAATAACCAA-3' and 5'-CCCGATGGTTCGGCATTGGATATATG-3'. The dCTR construct was obtained from multicopy insertions of primer oligonucleotides during d261CTR construction. These deletion constructs were purified with an EndoFree Plasmid Maxi kit (Qiagen, Hilden, Germany) and transfected in HeLa cells using Polyethylenimine MAX (PEI "MAX", Polysciences, Warrington, PA). After transfection, HeLa cells were cultured in DMEM supplemented with 10% fetal bovine serum in 5% CO_2 at 37°C for 48 h. The cells were then harvested for subcellular fractionation or subjected to fluorescence imaging using an inverted microscope, Axio Vert.A1FL-LED (Carl Zeiss).

Declarations

Acknowledgements

We thank Michihiro Igarashi, Akihide Koyama (Niigata University), and Tadashi Okubo (Kitasato University) for their helpful discussions, as well as Yukihiro Jimbo, Sachiko Hirokawa, Yoshitaka Yamamoto, Yoshitaka Maeda, Nobuyoshi Fujisawa (Niigata University), and Sadahiro Azuma (Kitasato University) for the management of the laboratory animal facilities. This work was supported by Grants-in-Aid for Scientific Research (JSPS KAKENHI) [grant numbers JP22590925, JP25461271, JP19K07848].

Author contributions

T.S. conceived of the study and wrote the manuscript with support from O.O.. T.S., K.O., S.S., R.K., S.Y., and M.I. performed the experiments. M.I., Y.K., M.N., T.S., and M.Y. analyzed the data. All authors reviewed the manuscript.

Additional Information

Competing interests: The authors declare no competing interests.

References

1. Ou, S. H., Wu, F., Harrich, D., Garcia-Martinez, L. F. & Gaynor, R. B. Cloning and characterization of a novel cellular protein, TDP-43, that binds to human immunodeficiency virus type 1 TAR DNA sequence motifs. *J. Virol.* **69**, 3584-3596, https://doi.org/10.1128/JVI.69.6.3584-3596.1995 (1995).

2. Tziortzouda, P., Van Den Bosch, L. & Hirth, F. Triad of TDP43 control in neurodegeneration: autoregulation, localization and aggregation. *Nat. Rev. Neurosci.* **22**, 197-208, https://doi.org/10.1038/s41583-021-00431-1 (2021).

3. Buratti, E. *et al.* Nuclear factor TDP-43 and SR proteins promote in vitro and in vivo CFTR exon 9 skipping. *EMBO J.* **20**, 1774-1784, https://doi.org/10.1093/emboj/20.7.1774 (2001).

4. Wu, L. S. *et al.* TDP-43, a neuro-pathosignature factor, is essential for early mouse embryogenesis. *Genesis* **48**, 56-62, https://doi.org/10.1002/dvg.20584 (2010).

5. Sephton, C. F. *et al.* TDP-43 is a developmentally regulated protein essential for early embryonic development. *J. Biol. Chem.* **285**, 6826-6834, https://doi.org/10.1074/jbc.M109.061846 (2010).

6. Kraemer, B. C. *et al.* Loss of murine TDP-43 disrupts motor function and plays an essential role in embryogenesis. *Acta Neuropathol.* **119**, 409-419, https://doi.org/10.1007/s00401-010-0659-0 (2010).

7. Neumann, M. *et al.* Ubiquitinated TDP-43 in frontotemporal lobar degeneration and amyotrophic lateral sclerosis. *Science* **314**, 130-133, https://doi.org/10.1126/science.1134108 (2006).

8. Arai, T. *et al.* TDP-43 is a component of ubiquitin-positive tau-negative inclusions in frontotemporal lobar degeneration and amyotrophic lateral sclerosis. *Biochem. Biophys. Res. Commun.* **351**, 602-611, https://doi.org/10.1016/j.bbrc.2006.10.093 (2006).

9. Ayala, Y. M. *et al.* TDP-43 regulates its mRNA levels through a negative feedback loop. *EMBO J.* **30**, 277-288, https://doi.org/10.1038/emboj.2010.310 (2011).

10. Polymenidou, M. *et al.* Long pre-mRNA depletion and RNA missplicing contribute to neuronal vulnerability from loss of TDP-43. *Nat. Neurosci.* **14**, 459-468, https://doi.org/10.1038/nn.2779 (2011).

11. Avendano-Vazquez, S. E. *et al.* Autoregulation of TDP-43 mRNA levels involves interplay between transcription, splicing, and alternative polyA site selection. *Genes Dev.* **26**, 1679-1684, https://doi.org/10.1101/gad.194829.112 (2012).

12. Bembich, S. *et al.* Predominance of spliceosomal complex formation over polyadenylation site selection in TDP-43 autoregulation. *Nucleic Acids Res.* **42**, 3362-3371, https://doi.org/10.1093/nar/gkt1343 (2014).

13. Koyama, A. *et al.* Increased cytoplasmic TARDBP mRNA in affected spinal motor neurons in ALS caused by abnormal autoregulation of TDP-43. *Nucleic Acids Res.* **44**, 5820-5836, https://doi.org/10.1093/nar/gkw499 (2016).

14. Sugai, A. *et al.* Robustness and vulnerability of the autoregulatory system that maintains nuclear TDP-43 levels: a trade-off hypothesis for ALS pathology based on in silico data. *Front. Neurosci.* **12**, 28, https://doi.org/10.3389/fnins.2018.00028 (2018).

15. Sugai, A. *et al.* Non-genetically modified models exhibit TARDBP mRNA increase due to perturbed TDP-43 autoregulation. *Neurobiol. Dis.* **130**, 104534, https://doi.org/10.1016/j.nbd.2019.104534 (2019).

16. Jiang, L. L. *et al.* Structural transformation of the amyloidogenic core region of TDP-43 protein initiates its aggregation and cytoplasmic inclusion. *J. Biol. Chem.* **288**, 19614-19624, https://doi.org/10.1074/jbc.M113.463828 (2013).

17. Mompean, M., Baralle, M., Buratti, E. & Laurents, D. V. An amyloid-like pathological conformation of TDP-43 is stabilized by hypercooperative hydrogen bonds. *Front. Mol. Neurosci.* **9**, 125, https://doi.org/10.3389/fnmol.2016.00125 (2016).

18. Hasegawa, M. *et al.* Phosphorylated TDP-43 in frontotemporal lobar degeneration and amyotrophic lateral sclerosis. *Ann. Neurol.* **64**, 60-70, https://doi.org/10.1002/ana.21425 (2008).

19. Neumann, M. *et al.* Phosphorylation of S409/410 of TDP-43 is a consistent feature in all sporadic and familial forms of TDP-43 proteinopathies. *Acta Neuropathol.* **117**, 137-149, https://doi.org/10.1007/s00401-008-0477-9 (2009).

20. Nonaka, T. *et al.* Phosphorylation of TAR DNA-binding protein of 43 kDa (TDP-43) by truncated casein kinase 1δ triggers mislocalization and accumulation of TDP-43. *J. Biol. Chem.* **291**, 5473-5483, https://doi.org/10.1074/jbc.M115.695379 (2016).

21. Nishino, K. *et al.* Mice deficient in the C-terminal domain of TAR DNA-binding protein 43 develop age-dependent motor dysfunction associated with impaired Notch1-Akt signaling pathway. *Acta Neuropathol. Commun.* **7**, 118, https://doi.org/10.1186/s40478-019-0776-5 (2019).

22. Winton, M. J. *et al.* Disturbance of nuclear and cytoplasmic TAR DNA-binding protein (TDP-43) induces disease-like redistribution, sequestration, and aggregate formation. *J. Biol. Chem.* **283**, 13302-13309, https://doi.org/10.1074/jbc.M800342200 (2008).

23. Ayala, Y. M. *et al.* Structural determinants of the cellular localization and shuttling of TDP-43. *J. Cell Sci.* **121**, 3778-3785, https://doi.org/10.1242/jcs.038950 (2008).

24. Nonaka, T., Kametani, F., Arai, T., Akiyama, H. & Hasegawa, M. Truncation and pathogenic mutations facilitate the formation of intracellular aggregates of TDP-43. *Hum. Mol. Genet.* **18**, 3353-3364, https://doi.org/10.1093/hmg/ddp275 (2009).

25. Wang, H. Y., Wang, I. F., Bose, J. & Shen, C. K. Structural diversity and functional implications of the eukaryotic TDP gene family. *Genomics* **83**, 130-139, https://doi.org/10.1016/s0888-7543(03)00214-3 (2004).

26. Schmidt, H. B., Barreau, A. & Rohatgi, R. Phase separation-deficient TDP43 remains functional in splicing. *Nat. Commun.* **10**, 4890, https://doi.org/10.1038/s41467-019-12740-2 (2019).

27. Kato, M. *et al.* Cell-free formation of RNA granules: low complexity sequence domains form dynamic fibers within hydrogels. *Cell* **149**, 753-767, https://doi.org/10.1016/j.cell.2012.04.017 (2012).

28. Conicella, A. E., Zerze, G. H., Mittal, J. & Fawzi, N. L. ALS mutations disrupt phase separation mediated by α-helical structure in the TDP-43 low-complexity C-terminal domain. *Structure* **24**, 1537-1549, https://doi.org/10.1016/j.str.2016.07.007 (2016).

29. Conicella, A. E. *et al.* TDP-43 α-helical structure tunes liquid-liquid phase separation and function. *Proc. Natl. Acad. Sci. U. S. A.* **117**, 5883-5894, https://doi.org/10.1073/pnas.1912055117 (2020).

30. Guenther, E. L. *et al.* Atomic structures of TDP-43 LCD segments and insights into reversible or pathogenic aggregation. *Nat. Struct. Mol. Biol.* **25**, 463-471, https://doi.org/10.1038/s41594-018-0064-2 (2018).

31. Loughlin, F. E. & Wilce, J. A. TDP-43 and FUS-structural insights into RNA recognition and self-association. *Curr. Opin. Struct. Biol.* **59**, 134-142, https://doi.org/10.1016/j.sbi.2019.07.012 (2019).

32. Shenoy, J. *et al.* Structural dissection of amyloid aggregates of TDP-43 and its C-terminal fragments TDP-35 and TDP-16. *FEBS J.* **287**, 2449-2467, https://doi.org/10.1111/febs.15159 (2020).

33. D'Ambrogio, A. *et al.* Functional mapping of the interaction between TDP-43 and hnRNP A2 in vivo. *Nucleic Acids Res.* **37**, 4116-4126, https://doi.org/10.1093/nar/gkp342 (2009).

34. Daoud, H. *et al.* Contribution of TARDBP mutations to sporadic amyotrophic lateral sclerosis. *J. Med. Genet.* **46**, 112-114, https://doi.org/10.1136/jmg.2008.062463 (2009).

35. Darling, A. L. & Uversky, V. N. Intrinsic disorder and posttranslational modifications: the darker side of the biological dark matter. *Front. Genet.* **9**, 158, https://doi.org/10.3389/fgene.2018.00158 (2018).

36. Gasset-Rosa, F. *et al.* Cytoplasmic TDP-43 de-mixing independent of stress granules drives inhibition of nuclear import, loss of nuclear TDP-43, and cell death. *Neuron* **102**, 339-357, https://doi.org/10.1016/j.neuron.2019.02.038 (2019).

37. Yu, H. *et al.* HSP70 chaperones RNA-free TDP-43 into anisotropic intranuclear liquid spherical shells. *Science* **371**, eabb4309, https://doi.org/10.1126/science.abb4309 (2021).

38. Pinarbasi, E. S. *et al.* Active nuclear import and passive nuclear export are the primary determinants of TDP-43 localization. *Sci. Rep.* **8**, 7083, https://doi.org/10.1038/s41598-018-25008-4 (2018).

39. Ederle, H. *et al.* Nuclear egress of TDP-43 and FUS occurs independently of Exportin-1/CRM1. *Sci. Rep.* **8**, 7084, https://doi.org/10.1038/s41598-018-25007-5 (2018).

40. Hashimoto, M. & Takemoto, T. Electroporation enables the efficient mRNA delivery into the mouse zygotes and facilitates CRISPR/Cas9-based genome editing. *Sci. Rep.* **5**, 11315, https://doi.org/10.1038/srep11315 (2015).

41. Itakura, M., Tsujimura, J., Yamamori, S., Ohkido, T. & Takahashi, M. NMDA receptor-dependent recruitment of calnexin to the neuronal plasma membrane. *Neurosci. Lett.* **550**, 173-178, https://doi.org/10.1016/j.neulet.2013.06.064 (2013).

42. Yamamori, S. *et al.* Differential expression of SNAP-25 family proteins in the mouse brain. *J. Comp. Neurol.* **519**, 916-932, https://doi.org/10.1002/cne.22558 (2011).

43. Yokoseki, A. *et al.* TDP-43 mutation in familial amyotrophic lateral sclerosis. *Ann. Neurol.* **63**, 538-542, https://doi.org/10.1002/ana.21392 (2008).

Figures

Fig. 1

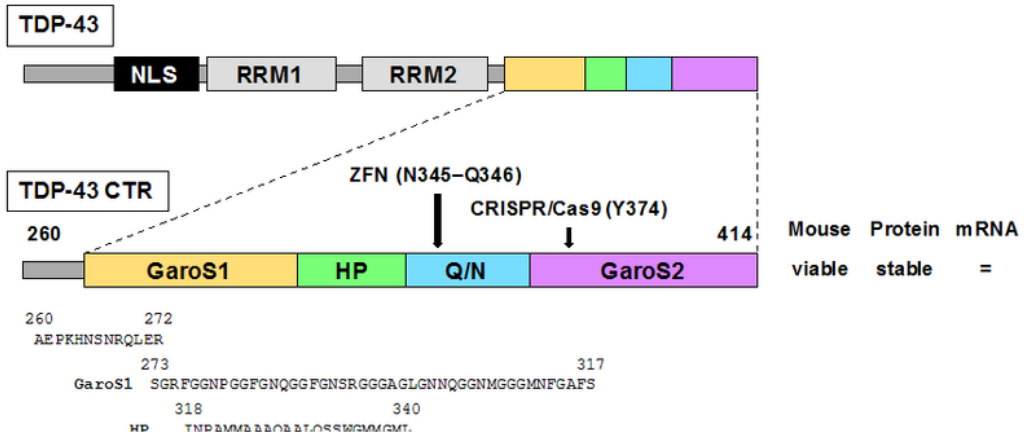

Figure 1

Schematic diagram of mouse TDP-43 and putative protein structures with various CTR deletions. TDP-43 contains 414 aa residues and consists of a bipartite nuclear localization signal (NLS), two RNA recognition motifs (RRM), and a long-disordered CTR. CTR is divided into four sub-regions, the GaroS1 (yellow), HP (green), Q/N-rich (blue), and GaroS2 segments (purple); the aa sequences are depicted by one-letter codes according to the TDP-43 CTR. The genome-edited mice were categorized into five groups

based on the putative CTR structures. Each deleted region is drawn as a red dotted line. The putative aa sequence in each mouse line is shown in black and red letters indicating WT and substituted aa residues, respectively. The gaps in the aa sequences are represented as red dashes. The characteristics of each group determined in this study are shown on the right. Mouse, embryonic lethality of homozygous mice. Protein, protein stability in the eight-week-old mouse cerebrum. mRNA, total expression level of the Tardbp mRNA. NE, not examined. Note that the putative protein structures of ZM93/Δ3 and ZM91/Δ1 mice (gray) are similar to those of ZM13A/Δ9 and ZE10/Δ10, respectively, and were not used in this analysis.

Figure 2

Western blotting and qRT-PCR analysis of the mice at eight weeks of age. (a, b, and c) Cytoplasmic (C), nuclear (N), and insoluble (I) fractions of cerebrum samples from Group 1 homozygous mice (a), Group 3 heterozygous and homozygous mice (b), or Group 4 and 5 heterozygous mice (c) were subjected to western blotting using the antibodies indicated on the right. Anti-α-tubulin and anti-p84 antibodies were used as loading controls for the cytoplasmic and nuclear fractions, respectively. Full-length blots are presented in Supplementary Fig. S4. (d and e) Quantification of λpolyA (external control) and Tardbp mRNA levels normalized to Hprt1 mRNA (internal reference). The total expression levels of Tardbp mRNA were evaluated using Exon 3–4 and Exon 5–6 primer sets. The WT Exon 6 primer set only recognized the WT allele. Each value indicates mean ± SEM as calculated by the REST2009 program. *$p < 0.05$, **$p < 0.01$.

Figure 3

Subcellular localization of non-functional TDP-43 lacking various CTR deletions, including the GaroS1-HP segment. (a) Immunohistochemical analysis of the spinal anterior horn region in WT and ZM39A/Δ261 mice stained with N-260 anti-TDP-43 antibody. Scale bar, 20 μm. (b, c, and d) Transient expression of EGFP-tagged human TDP-43 in HeLa cells. (b) Schematic diagram of human TDP-43 constructs lacking dGaroS1 (aa 262–317), d261CTR (aa 262–346), or dCTR (aa 262–414). (c) Fluorescence and phase contrast images of living cells. Scale bar, 20 μm. (d) Cytoplasmic (C) and nuclear (N) fractions of cell lysates were subjected to western blotting using the antibodies indicated on the right. Note that the blot with the EGFP antibody shows only the low molecular weight region (approximately 27 kDa). Full-length blots are presented in Supplementary Fig. S4.

Supplementary Files

This is a list of supplementary files associated with this preprint. Click to download.

- 20211125SupplToshiyaSatoR.docx